(4)

The Johns Hopkins University

MECHANISMS OF CREVICE CORROSION IN CHLORINATED ENVIRONMENTS

A FINAL TECHNICAL REPORT

SUBMITTED TO:

OFFICE OF NAVAL RESEARCH
ARLINGTON, VIRGINIA

RESEARCH CONTRACT #: N00014-87-K-0294
PROGRAM OFFICER: DR. A. JOHN SEDRIKS

SUBMITTED BY:

PATRICK J. MORAN, ASSOC. PROF.
BARBARA A. SHAW, PH.D.
DEPARTMENT OF MATERIALS SCIENCE AND ENGINEERING
THE JOHNS HOPKINS UNIVERSITY

JANUARY 1989

MECHANISMS OF CREVICE CORROSION IN CHLORINATED ENVIRONMENTS

A FINAL TECHNICAL REPORT

SUBMITTED TO:

OFFICE OF NAVAL RESEARCH
ARLINGTON, VIRGINIA

RESEARCH CONTRACT #: N00014-87-K-0294
PROGRAM OFFICER: DR. A. JOHN SEDRIKS

SUBMITTED BY:

PATRICK J. MORAN, ASSOC. PROF.
BARBARA A. SHAW, PH.D.
DEPARTMENT OF MATERIALS SCIENCE AND ENGINEERING
THE JOHNS HOPKINS UNIVERSITY

JANUARY 1989

PRELIMINARY INFORMATION

This final technical report presents the work conducted at The Johns Hopkins University over a two year period exploring the mechanisms of crevice corrosion in natural and chlorinated environments. The study concentrated on alloy 625 because of suspected crevice corrosion problems with this alloy in a highly oxidizing environment. The majority of the work was conducted by author Barbara A. Shaw who was at Hopkins on extended term training from the David Taylor Naval Ship R&D Center during the 1986-87 academic year. Barbara was able to find sufficient time to pursue this in addition to completing the coursework she proposed to obtain the leave. She combined this work with more applied work that she was involved in at David Taylor to present a Ph.D. thesis to Johns Hopkins. This report is a summary of that Ph.D. thesis and includes reference to four manuscripts which have been prepared from the work which are currently in review. As the first three manuscripts involved some aspect of the David Taylor work these were appropriately cleared with that agency prior to submission. There were no additional reports issued from this study. Those interested in obtaining copies of any of the manuscripts referenced should direct their inquiry directly to Pat Moran at Hopkins.

TABLE OF CONTENTS

INTRODUCTION

Crevice corrosion is considered by many to be the most deleterious form of corrosion because it occurs on shielded areas of a metal surface where visual examination of the underlying metal is difficult, if not impossible, and unpredicted catastrophic failures can result. Crevice corrosion has been observed on a variety of passive film forming metals[1-14] exposed in a number of different environments ranging from high purity water[2] to the human body[15]. This type of corrosion is inherent in metals and alloys that are easily passivated (e.g. stainless steels, aluminum and aluminum alloys, titanium and titanium alloys, and nickel base alloys), but also occurs on iron and mild steel exposed to highly oxidizing or passivating environments. Metal surfaces shielded by gaskets, washers, bolt heads, o-rings , barnacles or other surface deposits are typical sites for this type of corrosion.

In the early literature the concepts of differential aeration[16,17], metal ion concentration[15], inhibitor concentration[18,19], and hydrogen ion concentration

cells[20] were proposed to explain crevice corrosion. Each of these mechanisms advanced the understanding of the phenomena, but none were sufficient explanations by themselves. In the mid sixties Fontana and Greene combined two of these ideas into a unified mechanism[21] in order to explain the crevice corrosion of stainless steels in neutral pH environments containing chloride ions. This unified mechanism consists of 4 stages: 1) depletion of oxygen within the crevice, 2) increase in chloride ion content and acidity of the crevice solution, 3) permanent loss of passivity for the metal in the crevice, and, finally, 4) propagation of attack within the crevice. The first three steps constitute the initiation phase of crevice corrosion and the fourth step is propagation. Initially, the anodic reaction of slow alloy dissolution and the cathodic oxygen reduction reaction occur both inside and outside the crevice. In time, the oxygen within the crevice is depleted faster than it can be replenished by diffusion and the cathodic reaction moves outside the crevice where it can be supported by the higher dissolved oxygen content of the bulk solution. Slowly metal ions concentrate in the crevice and Cl- ions migrate into the crevice to maintain charge neutrality. Hydrolysis of metal chloride complexes in the crevice leads to the

formation of H+ ions; dropping the pH of the crevice solution. A point is eventually reached when the metal in the crevice becomes active and propagation of attack within the crevice ensues. At this stage, rapid dissolution of the metal inside the crevice is driven by the reduction reactions outside the crevice and, if thermodynamically possible, some hydrogen evolution inside the crevice.

Mathematical model results[22] reveal that step 1, depletion of oxygen within the crevice, occurs quickly requiring only a few minutes or less for crevice gaps on the order of several microns. Step 2 of the mechanism, increase in chloride ion content and acidity of the crevice solution, has also been well documented. For neutral pH bulk solutions, low pH values and high chloride ion concentrations within crevices have been reported by a number of investigators[23-26]. Chloride ion concentrations as high as 6.2 N and pH values as low as -0.13 have been documented for solutions removed from artificial pits (actually crevices) on 18Cr-16Ni-5Mo stainless steel[24]. Oldfield and Sutton determined that the critical crevice solution which forms inside alloy 625 crevices at initiation has a chloride ion content of approximately 6M and a pH of

0[27] or less[28]. Using a mathematical model developed by Gartland[29] it has been determined that even higher chloride ion concentrations and lower pH values are possible during the propagation stage of crevice corrosion. Much less has been reported concerning the third step in the mechanism, permanent loss of passivity within the crevice. Chloride ion induced breakdown and acidification are most often cited as the depassivation mechanisms responsible for the initiation of crevice corrosion. In this investigation an alternative depassivation mechanism for crevice corrosion initiation, involving the IR drop down a crevice, is presented. The mechanism is applicable to a variety of metals in a number of environments and examples utilizing data from the literature will be presented in the results section in order to explain the concept.

Crevice corrosion occurs most often in neutral pH environments containing chloride ions. Seawater is such an environment and the majority of cases of crevice corrosion described in the literature are concerned with the crevice corrosion of stainless steels in this environment. Initiation of crevice corrosion in seawater, or more precisely the

depassivation step in the initiation mechanism, is normally attributed to either chloride ion induced breakdown[30-33] or acidification[34,35].

For the chloride ion induced breakdown mechanism to be operative, the metal in the crevice must be polarized to a value where passivity is locally broken down; in other words, the breakdown potential, E_{bd}, for the metal in the aggressive crevice environment must be exceeded as shown in Figure 1. This is indeed a possibility in natural seawater where bacterial slime films form on metal surfaces and catalyze the oxygen reduction reaction; often shifting the open circuit potential for the metal several hundred millivolts in the positive direction over the course of a few days or weeks[36-40]. Depassivation of the metal within a crevice by a breakdown mechanism is also a distinct possibility in oxidizing environments such as chlorinated seawater. The oxidants present as a result of seawater chlorination have also been found to shift open circuit potential by several hundred millivolts[40-42].

In order for the acidification mechanism to be operative the passivating potential, E_{pp}, for the metal

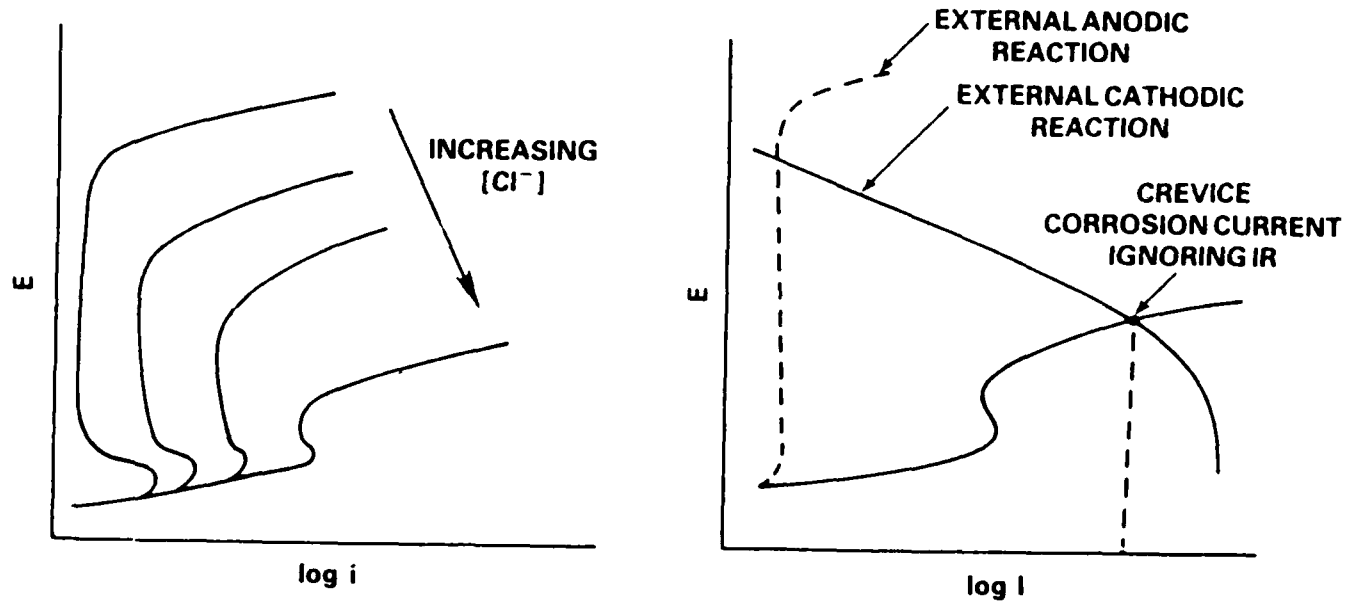

Figure 1 - Breakdown Mechanism for Crevice Corrosion Initiation

in the aggressive crevice environment must shift enough so that the mixed potential for the crevice couple is in the active nose of the anodic polarization curve as shown in Figure 2. A detailed description of the mechanism has been presented by Pickering[35]. In this report an additional depassivation mechanism, an IR induced mechanism, applicable to very corrosion resistant materials in neutral pH environments containing chloride ions will be presented and discussed.

Recent emphasis on using higher strength, more corrosion resistant alloys, such as highly alloyed stainless steels, nickel base superalloys and titanium in seawater handling systems for offshore applications and in marine cooling water systems has raised the issue of increased susceptibility of these materials to crevice corrosion in chlorinated seawater. Traditionally, copper based alloys have been used in these applications because of their inherent toxicity to marine biofouling. Unfortunately these more corrosion resistant materials possess no inherent toxicity to

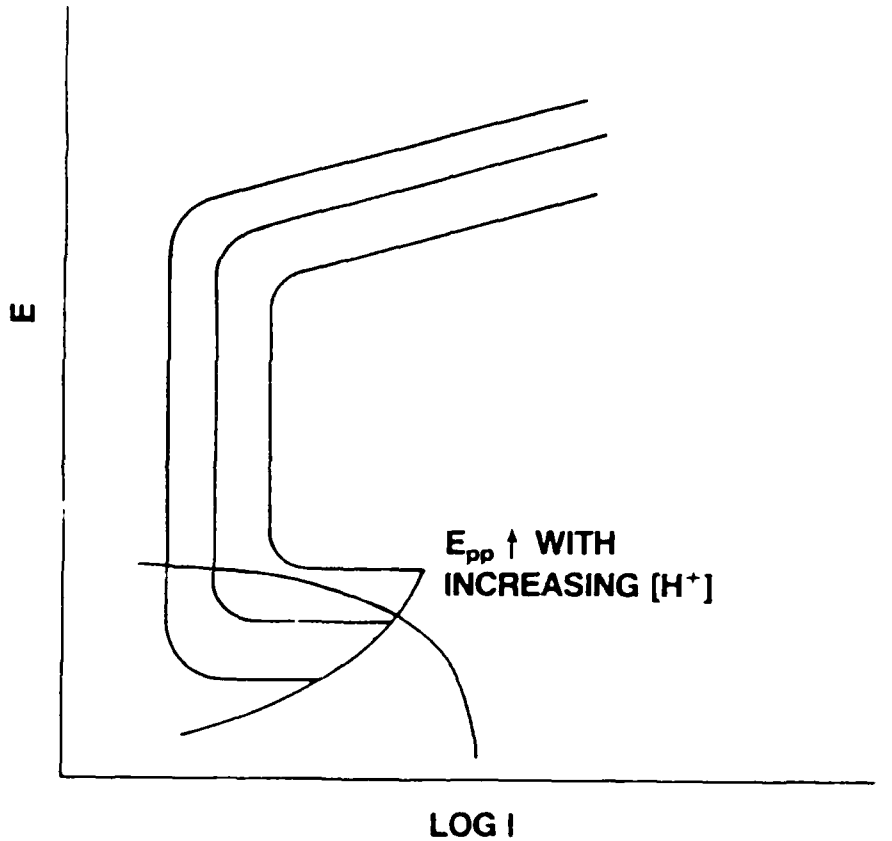

Figure 2 - Acidification Mechanism for Crevice Corrosion Initiation

marine biofouling and some means of controlling fouling is required if these materials are to be used in cooling water systems, firemains, and other piping systems where fouling control is essential. A number of oxidizing species are produced when seawater is chlorinated[43]. In low level chlorinated seawater (a few mg/l total residual oxidant or less) brominated species, primarily HOBr and OBr^-, predominate. In addition to the inactivation of marine micro and macro organisms, these oxidizing species are also responsible for the oxidation of metals. The oxidizing capability of chlorinated seawater has raised concern over increased susceptibility to localized corrosion especially, crevice corrosion, in these environments[32,40,42]. Increased incidences of crevice corrosion initiation have been observed for both stainless steels[32] and alloy 625[44] with chlorination. Chloride ion induced breakdown in the oxidizing chlorinated seawater has been speculated to be responsible the the increased incidences of crevice corrosion observed in chlorinated environments[32,45]. In contrast to this it has also been reported that crevice corrosion propagates at low rates in low level chlorinated seawater.

If crevice corrosion initiates relatively quickly, then it is the rate of propagation that determines the useful life of a material. The 4 step unified mechanism for crevice corrosion leaves the impression that initiation occurs by a breakdown mechanism (which is only one possibility) and that propagation is sustained by the maintenance of a high enough potential in the crevice to exceed the breakdown potential. However, there is considerable supporting evidence that crevice potentials are very low relative to the outside (cathode) potentials and that propagation actually occurs in the active nose of the anodic polarization curve. Negative potentials (with respect to those measured outside the crevice) have been measured inside iron, steel, stainless steel and titanium crevices. Greene et al.[46] documented potentials of less than -300 mV (vs. SCE) in a crevice formed on a 10Cr10NiFe alloy in 1N H_2SO_4 when the outside of the specimen was polarized at a potential of 1.6V. Pickering and Frankenthal[47] measured potential as a function of depth into an artificial pit/crevice on an iron specimen in a H_2SO_4 - Na_2SO_4 bulk environment (containing a small concentration of Cl^-) and measured potentials as low as -210 mV (vs. SHE) near the bottom of the crevice when the outer surface of the specimen was held at +840 mV

(vs. SHE). In both of these cases the potentials measured in the crevice corresponded with the active "nose" of the anodic polarization curve for these materials. Additional proof that crevice corrosion propagation occurs at active potentials has been reported by Kain and Lee[32] who observed negative shifts in the open circuit potentials of 316 and 18Cr-2Mo stainless steels with the onset of crevice corrosion. These results were obtained using a remote crevice configuration, of the type described by Lee[48]. Sharp increases in the current between the boldly exposed cathode and the shielded anode were measured coinciding with the electronegative shift in potential; confirming the initiation of crevice corrosion. Pickering and Frankenthal[47] and later Pickering and Valdes[49,50-52] documented the formation and evolution of H_2 in crevices, when thermodynamically impossible outside the crevice, providing further confirmation that a potential gradient exists within a crevice and is responsible for sustaining active dissolution. The results presented in this report provide additional support that crevice corrosion propagates at low potentials in the active nose of the anodic polarization curve.

The anodic dissolution of metal within the crevice is sustained by the cathodic reduction reactions occurring outside the crevice and possibly some hydrogen evolution within the crevice. In seawater the cathodic reaction of interest is oxygen reduction. If other oxidants are present, as in the case of chlorinated seawater, then the reduction of these species are also of interest. In seawater chlorinated at levels of a few mg/l or less total residual oxidant (TRO) it has been reported that crevice corrosion propagates at a lower rate than those observed in seawater[32,41]. This report identifies the role that chlorination plays in altering crevice corrosion propagation rates.

The objective of this investigation is to identify the mechanism responsible for crevice corrosion of a Ni-Cr-Mo-Fe alloy, alloy 625, in natural seawater and to determine the role that chlorination plays in altering crevice corrosion propagation. In order to accomplish this goal a three fold approach was taken:

1) simulated environments corresponding to those present during the initiation and propagation

stages of crevice corrosion were chosen based on mathematical model predictions, information in the literature and actual measurements;

2) steady state polarization behavior for alloy 625 in environments corresponding to those found inside and outside an active crevice was ascertained. Anodic polarization curves were generated in these simulated crevice environments and cathodic polarization curves were generated in natural seawater;

3) mixed potential theory, including the effects of IR drop down a crevice, was applied to the polarization data in order to identify the the crevice corrosion mechanism in natural seawater and to determine the role that chlorination plays in crevice corrosion propagation.

This investigation resulted in the compilation of four technical manuscripts. The major results of this work are presented and discussed in the following section. Following the results and discussion section is a section that details the overall conclusions of the research.

The first manuscript entitled "The Role of Ohmic Potential Drop in Crevice Corrosion - Part I: IR Induced Mechanism" and authored by Shaw and Moran (in review by Corrosion Science) addresses the concept of IR induced crevice corrosion and describes three distinct cases of how the IR drop down a crevice can initiate crevice corrosion using examples from the literature. The second manuscript entitled "The Role of Ohmic Potential Drop in Crevice Corrosion - Part II: Support for the IR Induced Mechanism" and authored by Shaw, Moran, and Gartland (in review by Corrosion Science) presents specific experimental results confirming an IR induced depassivation mechanism for crevice corrosion initiation on alloy 625 in a natural seawater environment. The third paper entitled "Resistance of Alloy 625 to Breakdown in High Chloride Crevice Environments" and authored by Shaw, Moran, and Gartland (in review by Corrosion Science) dispels the possibility of crevice corrosion initiation in chlorinated seawater as a result of chloride ion induced initiation. The fourth paper entitled "Crevice Corrosion Susceptibility of a Nickel Base Superalloy in Natural and Chlorinated Seawater" and authored by Shaw,

Moran, and Gartland (in review by Corrosion Science) examines crevice corrosion propagation for alloy 625 in natural and chlorinated seawater.

SUMMARY OF RESULTS AND DISCUSSION

IR Induced Mechanism for Crevice Corrosion Initiation

The majority of the literature concerned with crevice corrosion is unclear as to the exact depassivation mechanism involved in crevice corrosion initiation. In fact, the idea of IR induced depassivation has received little attention even though it may be the most common mechanism of crevice corrosion initiation for very corrosion resistant materials, for materials that exhibit high passive current densities, and for anodically polarized specimens. The concept of IR induced crevice corrosion will be presented in this section using examples derived from the literature. Specific experimental support for the mechanism in a bulk seawater environment will be presented and discussed in the next section. The importance of IR drop in crevice corrosion has been alluded to in the past[53,54] and a mechanism for pit/crevice propagation based on IR drop has been presented by Pickering and Frankenthal[48,55,56], but IR effects have not received focused attention as a predominate factor in crevice corrosion initiation. While Pickering[49,50] and Valdes and Pickering[51,52] have recently demonstrated the role

of IR in initiating and maintaining crevice corrosion on anodically polarized iron specimens, this section examines the importance of IR effects in crevice corrosion on a broader scale and includes a discussion of the results obtained by Pickering and Valdes.

Consider the example of a creviced iron specimen in a oxidizing acid such as concentrated HNO_3. Initially, the reduction of HNO_3 is responsible for the passivation of the metal surfaces inside and outside the crevice. The anodic and cathodic polarization behavior for the iron in the concentrated HNO_3 is presented in Figure 3a. In comparison to stainless steels, iron exhibits a high passive current density, on the order of 1 mA/cm^2, in 1 N H_2SO_4[57]. The dotted curve in Figure 3a reveals the underlying Evans diagram for the anodic polarization curve. Passivity of the metal outside the crevice is maintained by a fresh supply of HNO_3 to the metal surface. Inside the crevice, however, the supply of HNO_3 to the metal surface is impeded by the geometry of the crevice. In time, the HNO_3 within the crevice is reduced to HNO_2 and ultimately to NO[58]; diminishing the oxidizing capacity of the solution. As the oxidizing capacity of the crevice solution is reduced, the potential of the

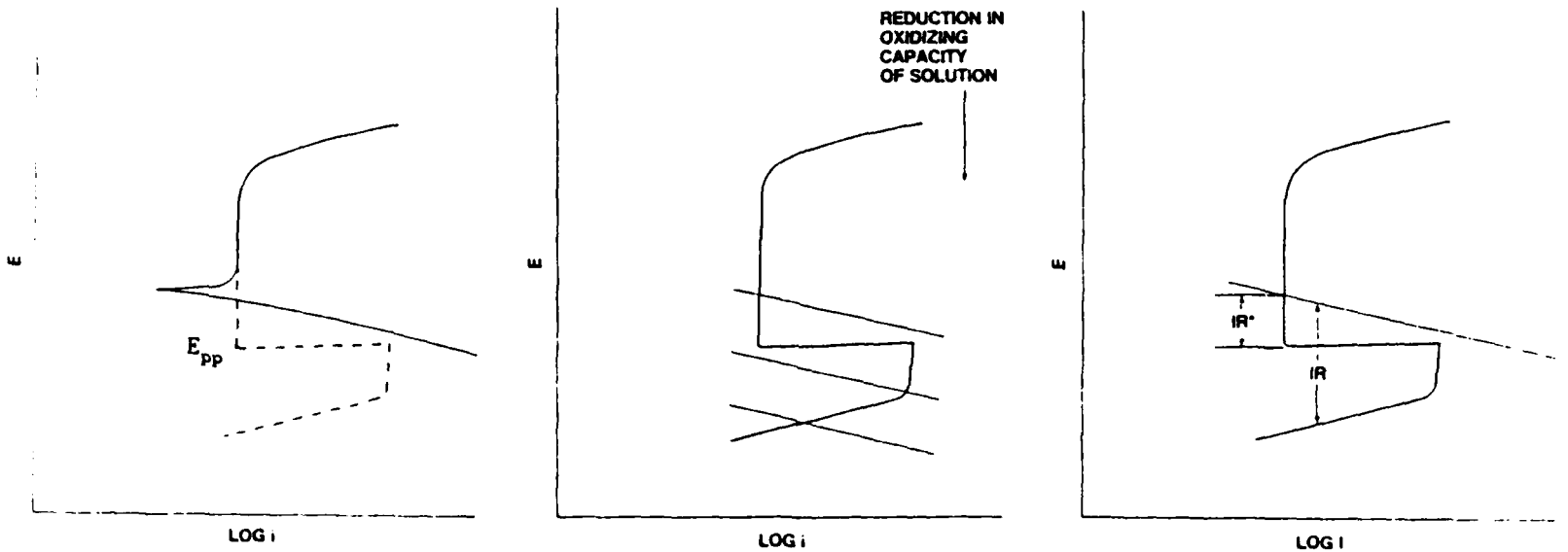

Anodic and Cathodic Polarization Curves for Iron in Concentrated HNO_3 (Dotted Curve Reveals Underlying Evans Diagram for Anodic Dissolution of Iron)

Evans Diagram for Iron in Acid Illustrating the Effect of Solution Oxidizing Capacity

Mixed Potential Analysis of Iron/Oxidizing Acid - Iron/Nonoxidizing Acid Crevice Couple

Figure 3 - IR Induced Crevice Corrosion - Iron in an Oxidizing Acid

iron in the crevice shifts in the negative direction as illustrated in Figure 3b. When the oxidizing power of the solution in the crevice is diminished to a value below the passivating potential, the iron in the crevice becomes active. This transition from passive to active is observed because of the loss of oxidant and the corresponding cathodic polarization of the metal in the crevice and not because the polarization characteristics of the metal have been altered.

The differences in the oxidizing capability of the solution inside and outside the crevice result in the formation of a "crevice couple" which can be evaluated using a mixed potential approach. Analysis of the "crevice couple" is made based on the current (I) rather than the current density (i) because the cathodic and anodic areas in a crevice situation are seldom equal. Superimposing the cathodic polarization curve in the bulk concentrated HNO_3 from Figure 3a on the anodic polarization curve for iron in the non-oxidizing concentrated acid environment within the crevice results in Figure 3c. If no crevice was present, the current at the cross-over point would represent the corrosion rate of the iron. When a

crevice is present, the high resistance of the narrow electrolyte path results in an IR drop along the length of the crevice. As long as the IR drop remains < IR^* crevice corrosion is not initiated. When the geometry of the crevice is such that $IR>IR^*$, the IR drop can no longer be accommodated in the passive region of the curve. The only region where the IR drop can be accommodated between the anodic and cathodic curves is in the active nose of the anodic curve. Thus, the IR drop is responsible for shifting the potential of the metal in the crevice to a region of active dissolution, initiating crevice corrosion. Once initiated, the IR drop maintains the potential of some portion of the crevice in the active nose of the anodic curve. The dimensions of the crevice will change with time and the region of the crevice with the highest rate of attack will shift depending on whether the crevice gap is widening or becoming clogged with corrosion product.

Another example of IR induced crevice corrosion involves crevice corrosion which occurs when an active-passive metal is anodically polarized. This form of crevice corrosion is sometimes referred to as "electrolytic crevice corrosion"[59,60]. Practical examples of electrolytic crevice corrosion include: crevice

corrosion which occurs when a metal is anodically polarized as a result of anodic protection[61], galvanic coupling, an electrolytic process or electrochemical experimentation[46]. In contrast to the case already described, crevice corrosion occurring under anodic polarization can occur instantaneously when current is applied to the specimen[15]. The only requirement for this form of crevice corrosion is a significant IR drop along the length of the crevice.

A crevice corrosion mechanism for this case has been described by Pickering[49,50], and Valdes and Pickering[51,52]. In their investigation, creviced iron specimens were potentiostatically held in the passive region at 600 mV (vs. SCE) and a clear acrylic plate was used to form a 10mm X 5mm X 0.5mm crevice over a portion of the iron specimen. The acetic acid electrolyte (pH=4.6) used in their experiments was buffered in order to discourage pH changes. Prior to anodic polarization the entire specimen was cathodically polarized in order to remove any air formed oxide. Once the specimen was anodically polarized, potential measurements were recorded along the length of the crevice. Increasingly negative potentials, with respect to the polarization potential, were recorded with

increasing depth into the crevice. Pickering and Valdes observed stable crevice corrosion without any further acidification of the crevice solution and without the presence of an aggressive species. Since the iron surface inside the crevice had already been activated prior to anodic polarization, deaeration of the crevice solution, while possible, was not a necessary condition for the establishment of stable crevice corrosion in these experiments. The only condition needed to establish and maintain stable crevice corrosion was the presence of a narrow electrolyte path resulting in an IR drop > IR^* along the length of the crevice, as illustrated in Figure 4. In addition to increasingly electronegative potentials in the crevice (with respect to the potential outside the crevice), visual observations of hydrogen formation within the crevice when it is not thermodynamically favorable outside the crevice, crystallographic morphology of attack in the crevice, and the presence of an active passive boundary inside the crevice provided proof that IR drop alone could be a necessary and sufficient condition for establishing crevice corrosion.

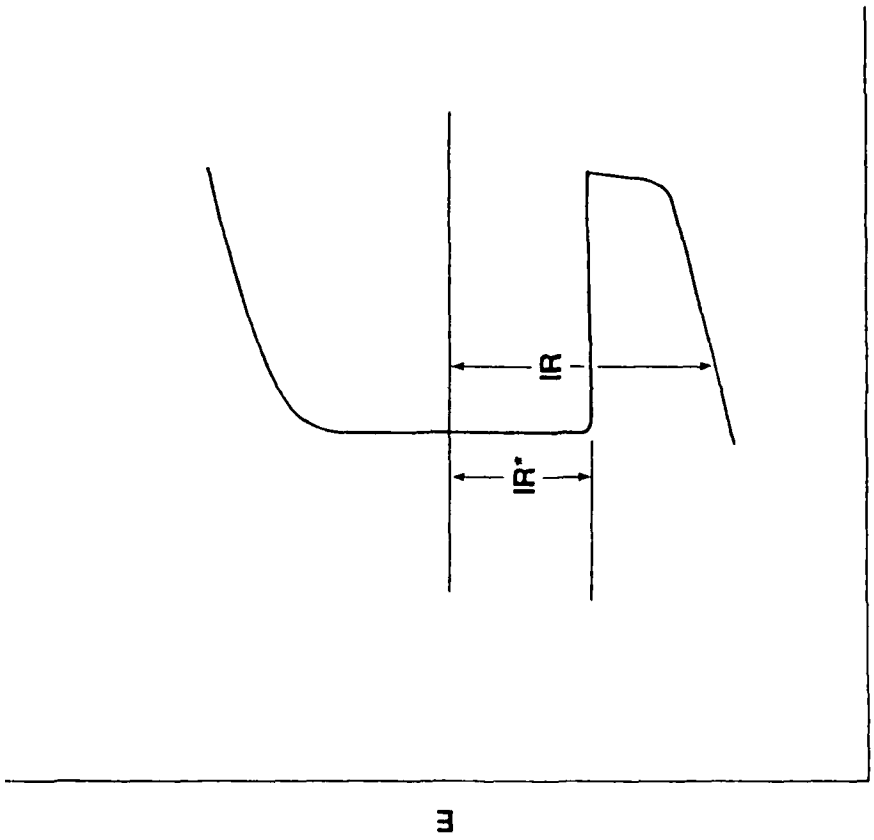

Figure 4 - IR Induced Crevice Corrosion - Iron in Buffered Acetic Acid Under Anodic Polarization

Crevice Corrosion in Natural Seawater

Alloy 625 is a high strength, corrosion resistant material that is being used increasingly by the chemical and power industries in environments where stainless steels suffer severe localized corrosion. The excellent uniform corrosion resistance of this alloy in seawater is well documented[62-66]. Alloy 625 also exhibits excellent resistance to pitting[62,67], but has been found to be susceptible to crevice corrosion in seawater[31,41,68,69] when tight crevices are present. A crevice corrosion initiation mechanism for alloy 625 in natural seawater, involving the IR drop down the crevice, will be presented in this section and crevice corrosion propagation will be discussed thereafter. Mixed potential theory will be used to illustrate the crevice corrosion mechanism. Anodic polarization behavior in two simulated crevice solutions will be used in the analysis. The first solution corresponds to the chemistry within the crevice when crevice corrosion first initiates. Artificial seawater saturated with NaCl ($[Cl^-]$ 6M), acidified to a pH of -0.25 and deaerated with nitrogen was chosen based on mathematical model results of Oldfield and Sutton.

During the early stages of propagation the acidity and chloride ion content of the crevice solution continues to increase and finally after a period of time steady state conditions are established. The chemistry of the second solution corresponds to one that would be found at some time during the propagation stage. An 8.18 M chloride solution with a pH of -1.2 was chosen for these experiments. The cathodic polarization data was generated both before and after long term exposure of crevice free specimens in natural seawater. Additional details on the experimental procedure and supplementary background information are available in the manuscripts.

Several investigators [36-40], have reported positive shifts in the open circuit potentials for metals exposed to natural seawater. The positive shift in open circuit potential with time has been attributed to bacterial slime films which form on metal surfaces in natural water environments. The exact mechanism by which the slime film enhances reduction kinetics of dissolved oxygen in seawater is still under investigation[39], but it has been hypothesized that either an increase in the exchange current density for the oxygen reduction reaction or a decrease in the cathodic Tafel

constant are responsible. An open circuit potential versus time curve for alloy 625 in quiescent, natural seawater (Wrightsville Beach, NC, temperature ranged from 16 to 18 C) is presented in Figure 5. Additional experimental details are available in the second manuscript. The potential shifts positively in stages with the first plateau occurring at approximately 50 mV (vs. SCE) and a later plateau occurring at 150 to 200 mV. In a related investigation[70], Kain observed initiation of crevice corrosion on creviced cylindrical alloy 625 pipe specimens after 18 to 20 days of exposure to flowing natural seawater (Wrightsville Beach, NC, flow rate = 1 m/s, mean water temp. 14.8 C). This time coincides with the first plateau in potential observed on the open circuit potential vs. time curve at 50 mV (vs. SCE). Kain's data establish that 18 to 20 days are necessary in order to develop a crevice solution aggressive enough to initiate crevice corrosion. From the open circuit potential measurements obtained under almost identical conditions it can be see that the open circuit potential for alloy 625 in natural seawater is approximately +50 mV (vs. SCE) at the time of initiation. Cathodic polarization curves generated after 2 hours, 13 days and 25 days of exposure to natural seawater (temperature ranged from

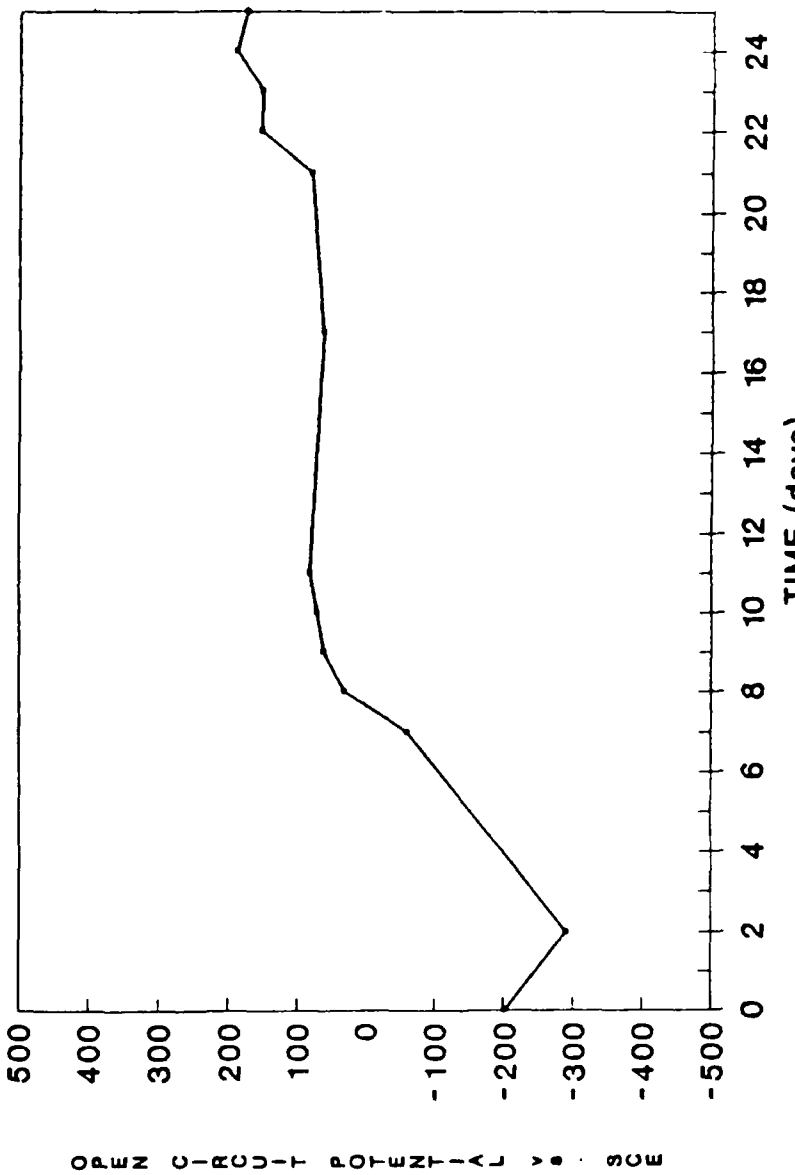

Figure 5 - Open circuit Potential vs. Time Behavior for Alloy 625 in Natural Seawater (Wrightsville Beach, Water Temperature 16 to 13°C)

16 to 13 C) are presented in Figure 6. Again, these specimens were exposed in the same location and at the same time of year as the ones used in Kain's study. These curves clearly illustrate the positive shift in open circuit potential with slime film formation and also reveal that the slime film does not effect the diffusion controlled portion of the reaction. It will be shown that this positive shift in potential plays a significant role in both the initiation and propagation stages of crevice corrosion.

The steady state anodic polarization behavior of alloy 625 in a solution representative of the chemistry present at the time crevice corrosion initiates is presented in Figure 7. Additional experimental details of these experiments are available in the second manuscript. For comparison the anodic polarization behavior of alloy 625 in deaerated artificial seawater (pH=8.2, [Cl-]=0.5M), generated in the same manner as the curve in the simulated crevice environment, is also shown in this figure (dashed line). In seawater alloy 625 is self passivating and exhibits two regions of passivity before the onset of transpassive dissolution at potentials greater than +800 mV (vs. SCE). In the

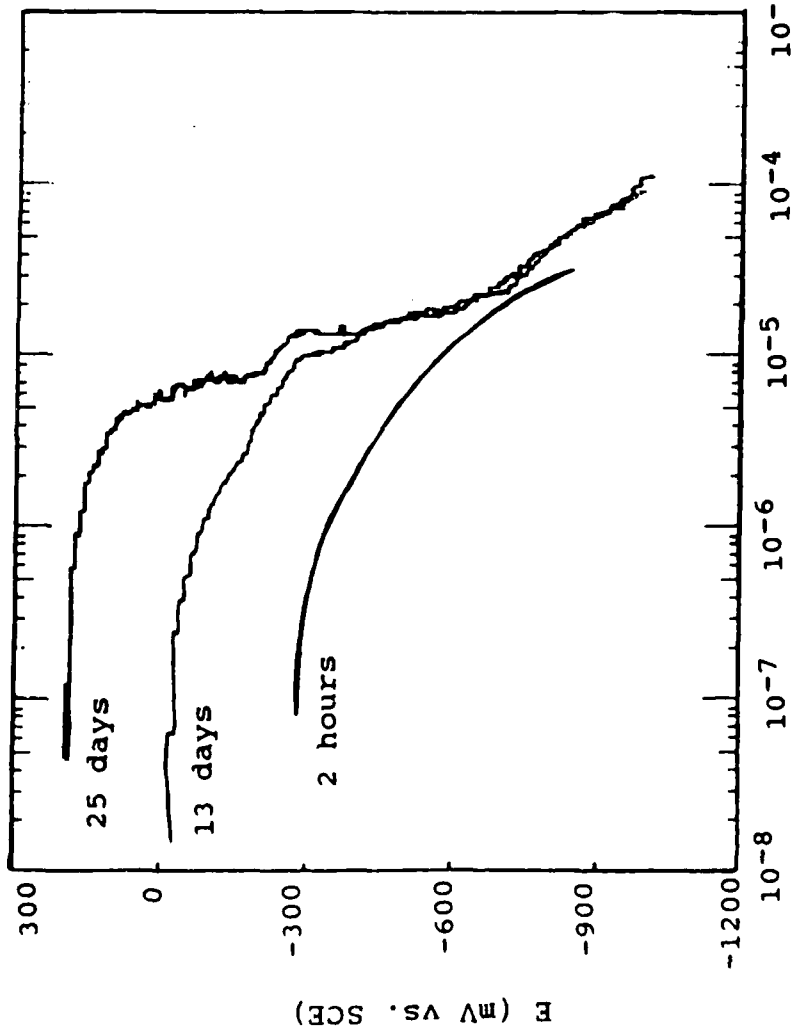

Figure 6 - Cathodic Polarization Behavior for Alloy 625 after 2 Hours, 13 days and 25 days of Pre-exposure in Natural Seawater (Water Temperature 16 to 13°C).

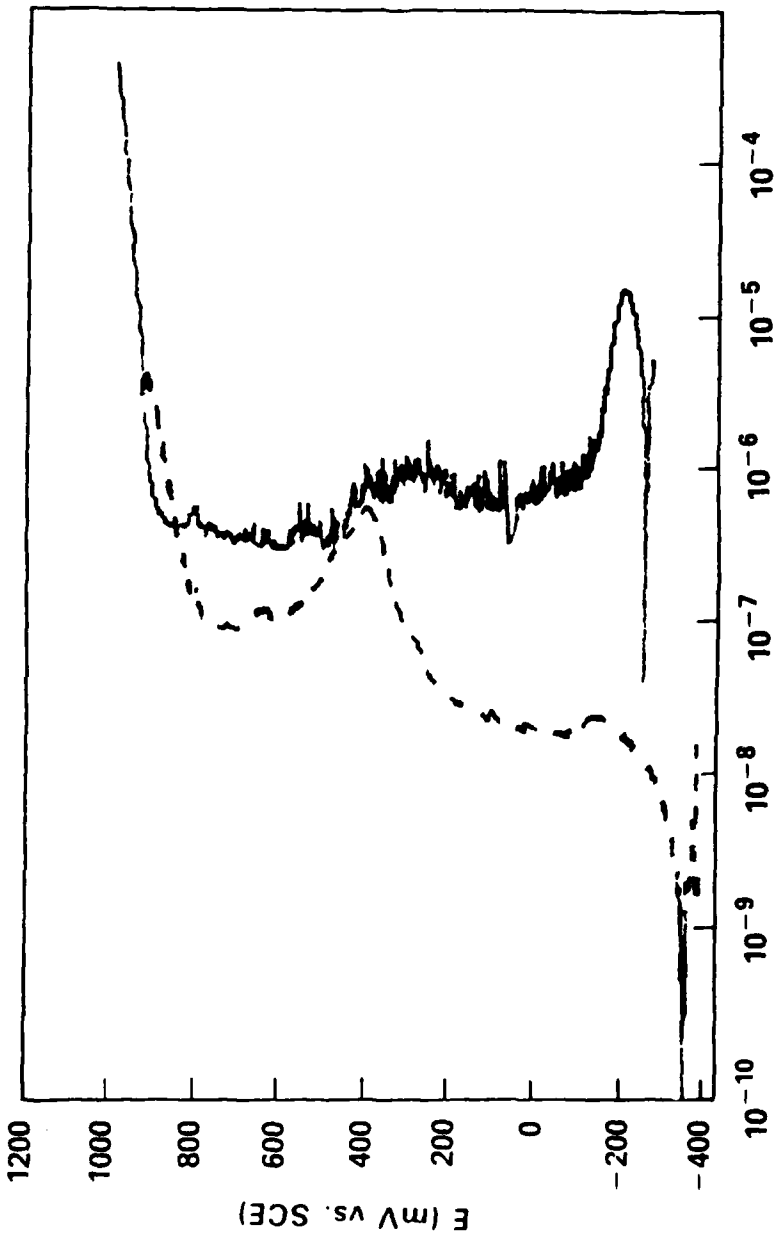

Figure 7 - Anodic Polarization Behavior of Alloy 625 in Simulated Crevice Solution at Crevice Corrosion Initiation (For Comparison Polarization Behavior in Artificial Seawater is Presented - Dashed Curve).

simulated crevice environment (pH=-0.25, saturated with NaCl, o=4.5 ohm-cm) a small active passive "nose" is observed in the anodic polarization curve. The active nose is visible in the simulated crevice solution and not in the neutral pH artificial seawater because the passivating potential shifts positively as the pH of the solution decreases[71,72]. A broad range of passivity was noted between -100 mV and 900 mV in the simulated crevice solution before the onset of transpassive dissolution at approximately 900 mV. The passive current density was found to be potential dependent, increasing a little more than half an order of magnitude over the 1 V passive range. This dependence of i_{pass} on potential is commonly observed in nickel[73] and nickel containing alloys. Note that the passive current density in the simulated crevice environment is 1 to 1.5 orders of magnitude higher than the passive current density in seawater.

Figure 8 shows the cathodic polarization curve for alloy 625 after 13 days of exposure to natural seawater (from manuscript 4) adjusted for an area of 100 cm^2 and

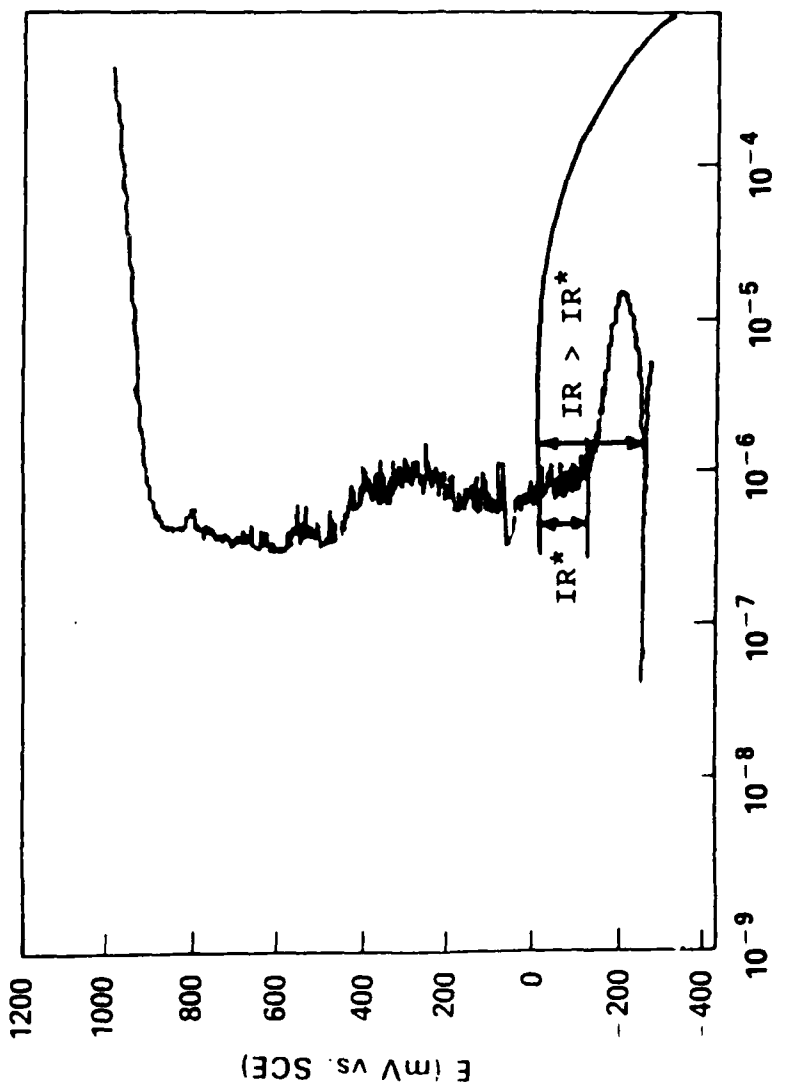

Figure 8 - Mixed Potential Analysis of Crevice Couple in Natural Seawater Illustrating IR Induced Crevice Corrosion

superimposed on the anodic polarization curve in the simulated crevice environment. This cathodic curve was chosen because it coincides most closely with the potential at the time crevice corrosion initiates[a]. This analysis assumes that the slime film shifts the open circuit potential positively prior to the development of the anodic curve pictured in Figure 8. This assumption is supported by Kain's observation that 18 to 20 days were required for crevice corrosion initiation of alloy 625 when the mean water temperature was 14.8 C. Analysis of the "crevice couple" is based on current rather than current density because the anodic and cathodic areas are not equal. If the IR drop down the crevice is negligible, the cross over point for the two curves would represent the corrosion rate in the crevice at the time of initiation. In most cases however, the IR drop associated with the restricted geometry of a crevice is not negligible and must be accounted for in the mixed potential analysis.

---

[a] In the second manuscript cathodic polarization behavior after 25 days instead of 13 days was used because at the time the manuscript was written it was unclear exactly when initiation occurred. Subsequently 13 days was determined, as mentioned previously, and is, therefore, presented here. The mechanism is the same regardless of whether the 13 or the 25 day data are used.

In order to demonstrate how IR drop induces depassivation of the metal within the crevice and initiates crevice corrosion, consider a crevice 1 cm long by 1 cm wide with a 0.2 u gap between the metal and the crevice former. This gap is typical of the gap that exists when a deformable material, such as an o-ring, is pressed against a metal surface[74]. A 225,000 ohm resistance is calculated using the 4.5 ohm-cm resistivity measured for the simulated solution and the dimensions listed. Recall that the passive current density in the simulated crevice solution at the time crevice corrosion initiates is 1 to 2 orders of magnitude higher than the passive current density in seawater. Combining the 225,000 ohm resistance of the crevice and the cross-over current density for the anodic and cathodic curves results in an IR drop of 180 mV. This IR drop is larger than IR*, the IR drop which can be accommodated between the two curves in the passive region of the anodic polarization curve as illustrated in Figure 8. As a result, the IR drop causes the metal within the crevice to reside at a potential in the active nose of the anodic polarization curve. At this potential the passive film is no longer stable and active dissolution of the metal initiates crevice corrosion.

After initiation and before steady state propagation the acidity and chloride ion content of the crevice solution continue to increase[29]. The aggressiveness of the crevice solution used in the propagation experiments was altered by increasing the chloride ion content to 8.18 M and decreasing the pH to -1.2; these values where chosen based on results from a mathematical model developed by Gartland[29]. Figure 9 illustrates the evolution of the anodic polarization curve with increasing chloride ion content and decreasing pH. This figure shows that in the 8.18 M chloride solution with a pH of -1.2 a very large active nose is present in the anodic polarization curve. The active nose extends over the first 600 mV of the polarization curve and current densities as high as 1×10^{-2} A/cm^2 are observed.

Again, a mixed potential approach will be utilized to evaluate the role that the cathodic reactions play in driving crevice corrosion propagation and also to estimate the crevice corrosion propagation rate. Figure 10 shows the "crevice couple" formed by the cathodic polarization curve in a bulk natural seawater environment after 25 days and an anodic curve generated

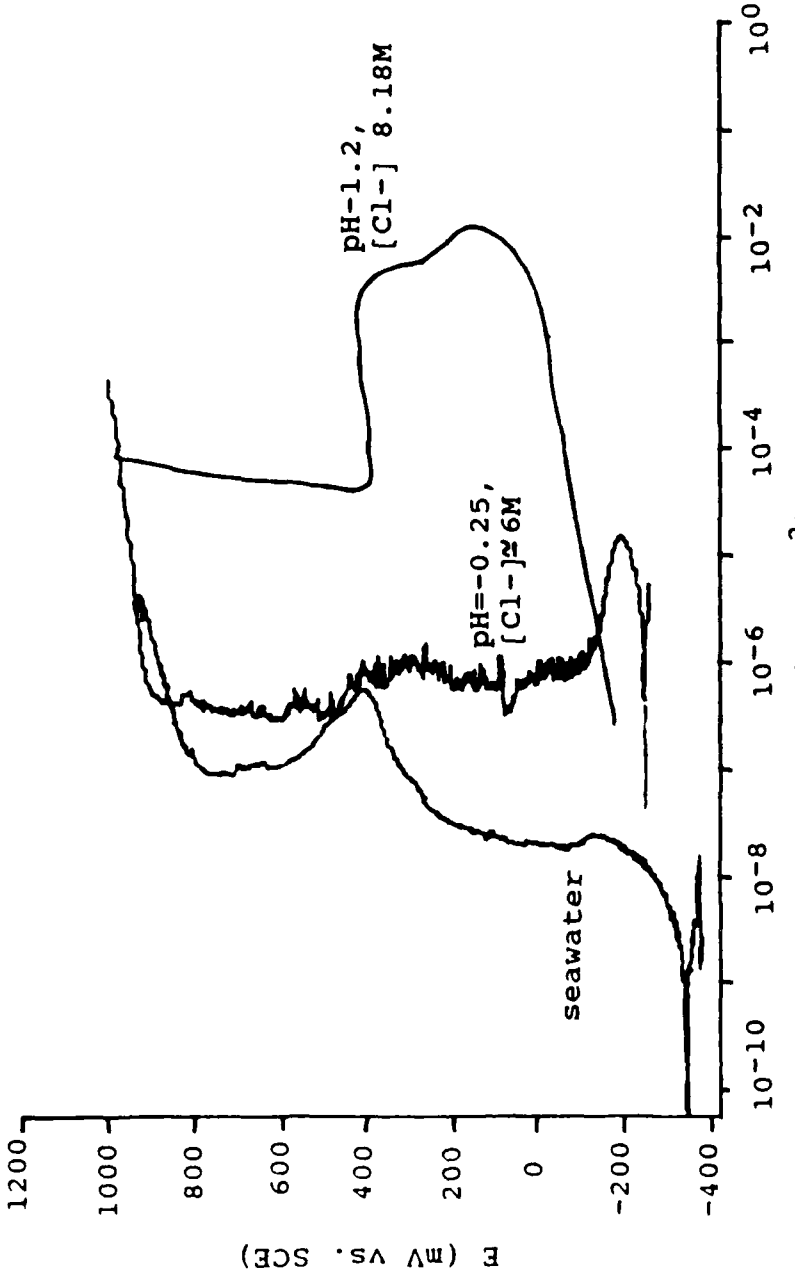

Figure 9 - Evolution of Anodic Polarization Curve with Decreasing pH and Increasing Chloride Ion Concentration

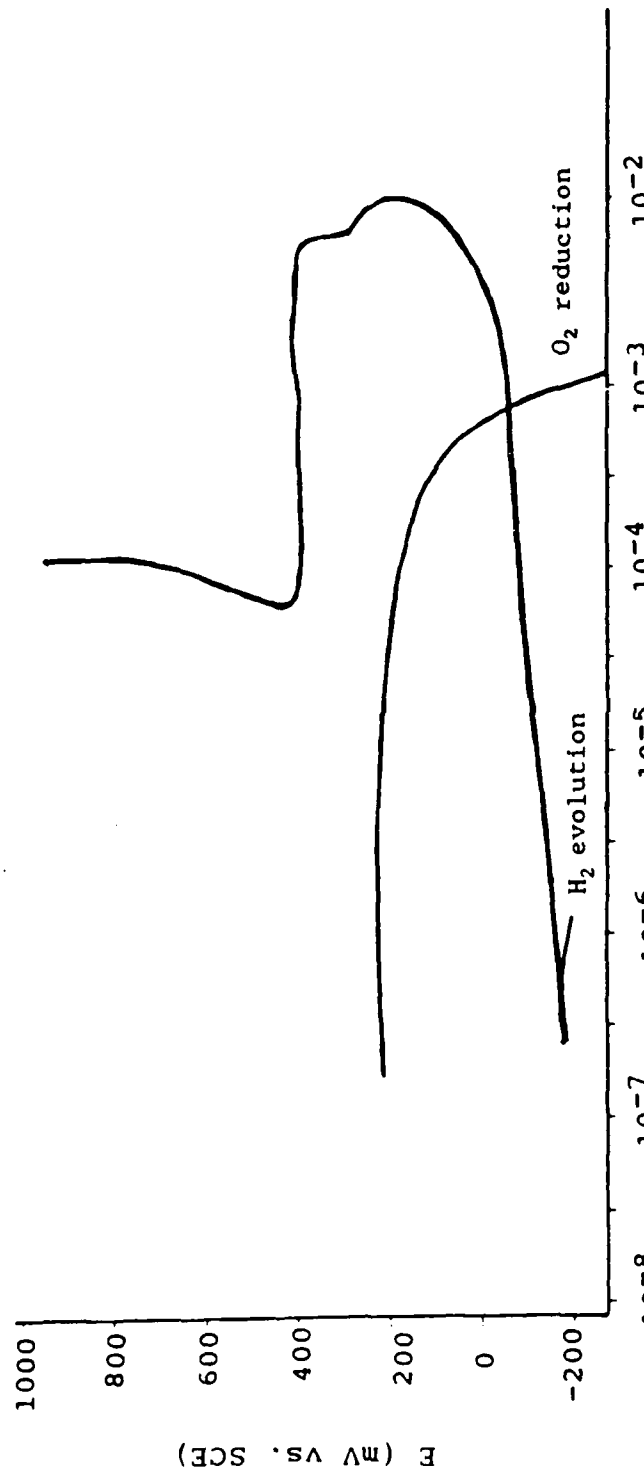

Figure 10 - Mixed Potential Analysis of Crevice Couple in Natural Seawater During Propagation Stage

in a simulated crevice solution corresponding to the more aggressive conditions present during crevice corrosion propagation. Specific details of this experiment are in manuscript 4. A cathode to anode area ratio of 100 to 1 is, again, considered. This figure shows that the diffusion limited portion of the cathodic oxygen reduction reaction crosses the large active nose of the anodic curve at a current of approximately 1 X 10^{-3} A/cm^2. The cathodic hydrogen evolution reaction in the crevice environment crosses the anodic curve at a current several orders of magnitude lower than the cross over current for the oxygen reduction reaction and, therefore, does not play a significant role in crevice corrosion propagation. During the propagation stage the IR drop down the length of the crevice is beneficial and propagation would be reduced with increasing depth into the crevice. Figure 11 illustrates the effects of IR drop on crevice corrosion propagation; using a crevice solution resistivity of 4.5 ohm-cm(see manuscript 2), crevice width of 1 cm and a crevice gap of 1 u. As the depth into the crevice is increased from 0.01 cm to 0.4 cm the current in the crevice is found to decrease from a value of 3 X 10^{-4} to 2 X 10^{-5} A.

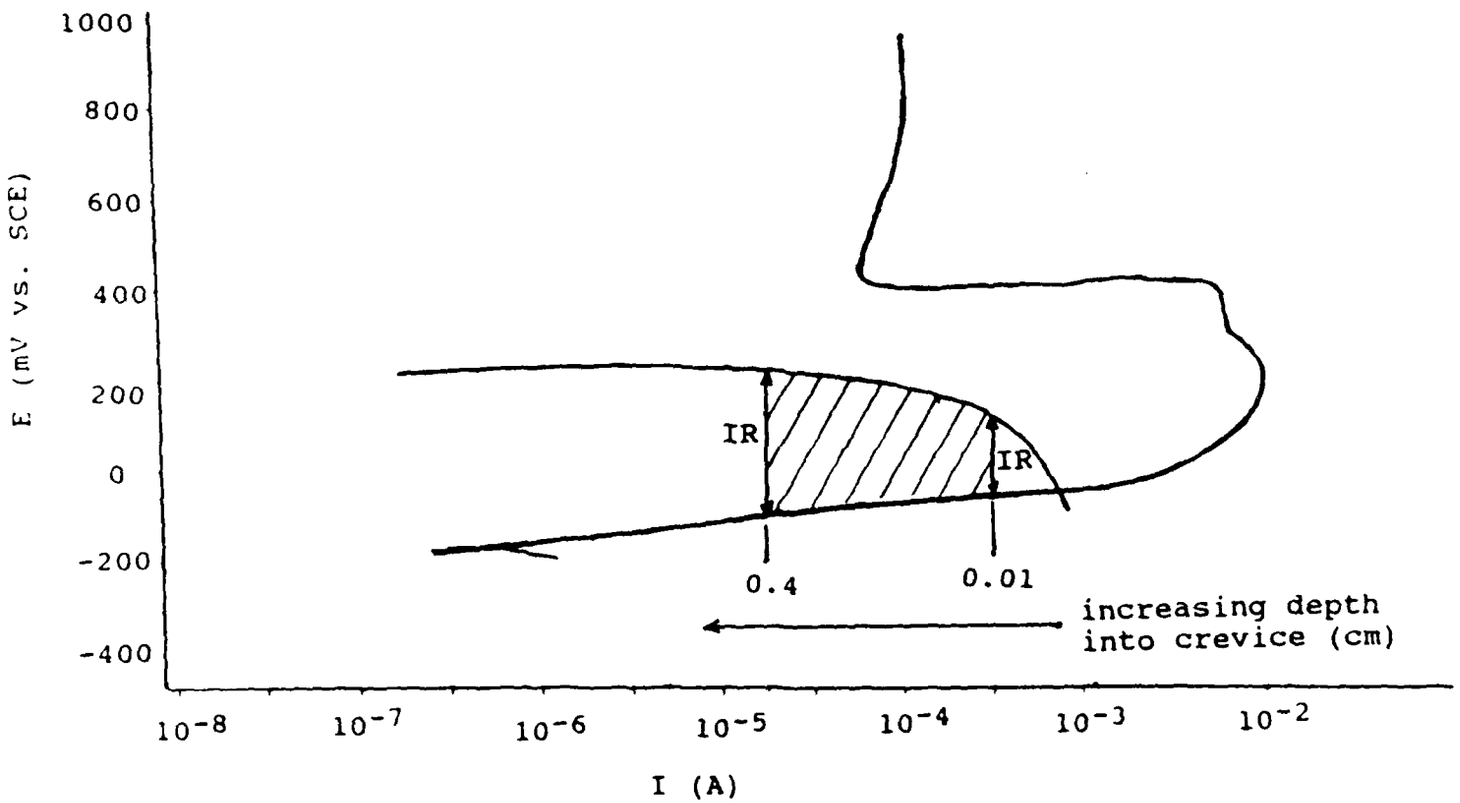

Figure 11 - Mixed Potential Analysis of Crevice Couple in Natural Seawater During Propagation Stage Including the Effects of IR Drop Down the Crevice

In a related investigation[70] Kain estimated a propagation current density of 21 uA/cm^2 for a creviced alloy 625 specimen (crevice gap approximately 1 u) after 40 days of exposure to natural seawater flowing at 1 m/s using a remote crevice specimen configuration. The actual attacked crevice area in Kain's investigation was 3.2 cm and a cathode to anode area ratio of 3.9 to 1 was used. The mixed potential analysis estimate can be compared to this data once the effect of flow on Kain's data has been established and subtracted out. This estimate can be made by comparing Kain's current density with the limiting current density for the oxygen reduction reaction under static conditions from Figure 6. Based on a limiting current density of 1 X 10^{-5} for oxygen reduction under static conditions it appears that the 1 m/s flow is responsible for approximately doubling the limiting current density. Reducing Kain's current density by one half and multiplying this value by the area and by a factor of 25, to account for the larger cathode considered in the mixed potential analysis, results in a current of 8.37 X 10^{-4}. This value is in fairly close agreement with the mixed potential estimates presented in Figure 11. If a cathodic curve generated

in artificial seawater had been used instead of the cathodic curve generated in natural seawater the crevice couple presented in Figure 12 would have resulted. In the artificial environment the activation controlled portion of the oxygen reduction reaction crosses the anodic curve instead of the diffusion controlled portion of the curve resulting in an large underestimation of crevice corrosion propagation rates.

Mixed potential analysis of the anodic and cathodic polarization curves representative of those found inside and outside an actively propagating crevice revealed the importance of acidification and increased chloride ion concentration in establishing the large active nose in the anodic polarization curve. Crevice corrosion is driven by the diffusion of oxygen to the outside (cathodic) surface, but the development of this large active region establishes the possibility for very high propagation rates if the cathode area is increased or if flow to the cathode is increased. IR drop plays a beneficial role in the propagation stage of crevice corrosion because it limits propagation rates with increasing depth into the crevice. If truly representative environments are chosen to model the solutions present inside and outside the crevice, then

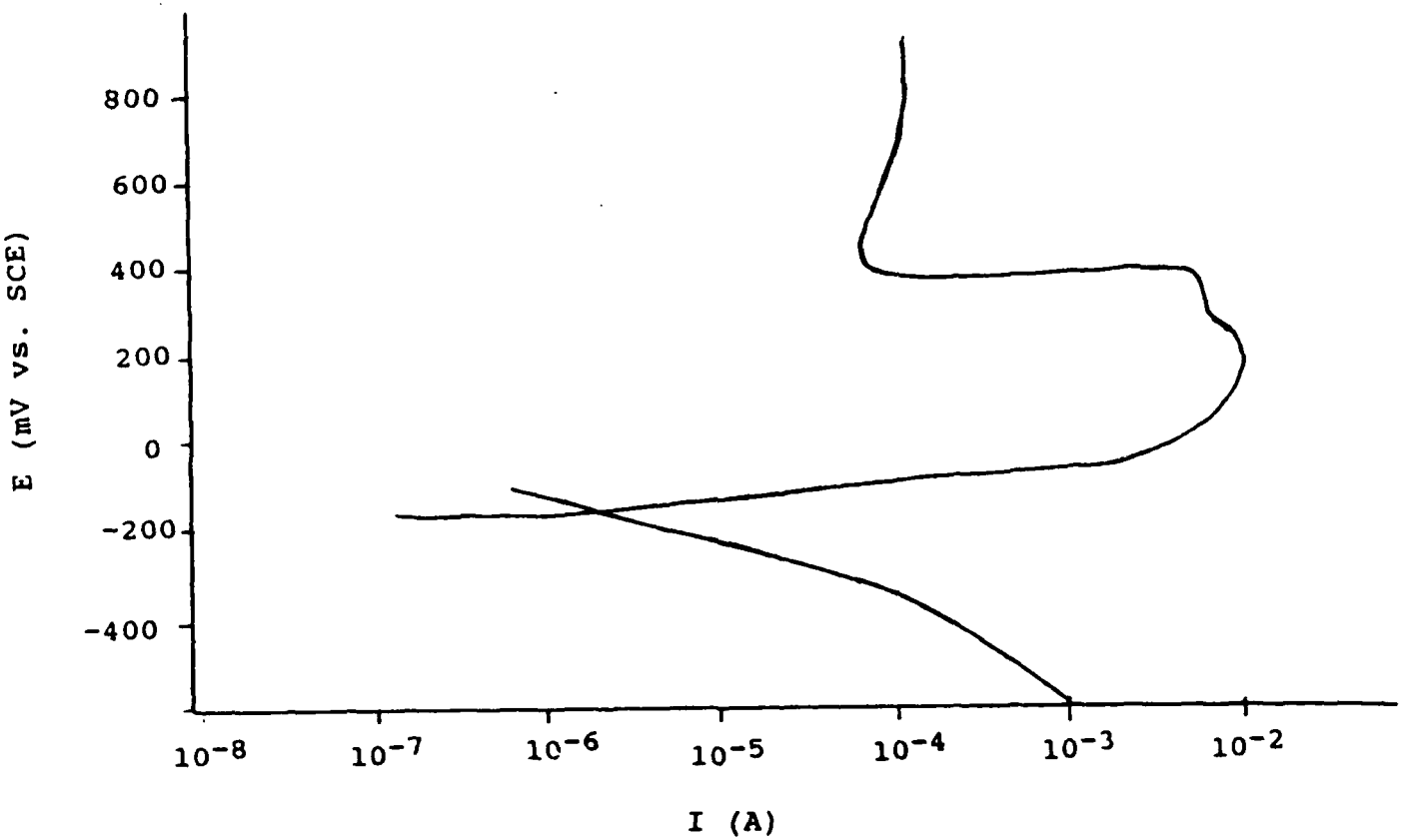

Figure 12 - Mixed Potential Analysis of Crevice Couple in Artificial Seawater During the Propagation Stage

crevice corrosion rates can be estimated using mixed potential theory. Finally, this analysis emphasizes the need to use a biologically active environment when evaluating the oxygen reduction reaction or determining corrosion rates in a seawater environment.

Crevice Corrosion in Chlorinated Seawater

The use of nickel base superalloys in chlorinated seawater cooling systems of power plants, oil refineries and offshore oil platforms has raised concern over the susceptibility of these alloys to crevice corrosion in oxidizing chlorinated seawater environments. Of specific interest are the possibility of crevice corrosion initiation by a chloride ion induced breakdown mechanism at the high potentials generated in chlorinated environments and the effect of low level chlorination (1 mg/l) in reducing crevice corrosion propagation rates[32,40,42]. Seawater chlorination results in the production of a number of oxidants the composition and concentration of which depend on temperature, pH and chlorination level. A review of seawater chlorination chemistry is presented in the third manuscript. The primary oxidants present

in open ocean water at low chlorination levels (a few mg/l or less total residual oxidant) are HOBr and OBr^-. Chlorination levels of a few mg/l total residual oxidant (TRO) or less are typical in fouling controlled seawater systems. Higher chlorination levels (65 to 100 mg/l total residual oxidant) can be encountered as effluent from an electrolytic chlorinator in a fouling controlled seawater piping system. At these higher chlorination levels HOCl and OCl^- are present in addition to the HOBr and OBr^-. In either case these oxidants are responsible for high open circuit potentials measured on alloy 625 in chlorinated seawater. Open circuit potentials of approximately 300 mV (vs. SCE) are quickly established in seawater chlorinated to a level of 1 mg/l TRO and potentials of 800 mV are quickly established at chlorination levels of 100 mg/l TRO. The crevice solution chemistries at initiation and during propagation are assumed to be the same as those presented in the natural seawater section. The small amount of oxidant present within the crevice is assumed to be quickly reduced and the resulting additional chloride ions are insignificant in comparison to the 0.5 M chloride solution initially present within the crevice. The reader is referred to

manuscripts 3 and 4 for additional background information and specific details of the experimental procedure.

Potentiodynamic polarization curves generated in the simulated crevice solution at initiation revealed no signs of chloride ion induced breakdown for alloy 625. These curves were generated at a very slow scan rate, 0.005 mV/s, requiring approximately 3 days for the generation of each curve. In order to confirm that breakdown did not occur with long term exposure to high chloride solutions eighteen day potentiostatic polarization experiments were conducted in an 8 M Cl^- solution at the highest possible potential attainable at the chlorination levels investigated in this research ,+800 mV. Low steady state current densities of 0.7 to 3.4 uA/cm^2 were observed over the course of the 18 days and SEM analysis of the specimen surface at the end of the test revealed no breakdown of the passive film; proving that crevice corrosion of alloy 625 does not initiate by a breakdown mechanism. Mixed potential analyses of the crevice couples formed in both high and low level chlorinated seawater point to initiation of crevice corrosion by either an IR induced mechanism or an acidification mechanism.

Since crevice corrosion of alloy 625 in chlorinated seawater initiates relatively quickly (a number of hours to a number of weeks depending on the bulk environment[75]) the propagation stage is of much greater engineering significance than the initiation stage. As was stated earlier, crevice corrosion propagation is driven by the reduction reaction(s) occurring in the bulk environment and possibly some hydrogen evolution within the crevice. Cathodic polarization curves generated in low level chlorinated seawater reveal that the primary cathodic reactions in the potential range of interest from +300 to -300 mV result from the reduction of HOBr and OBr^- (see manuscript 3 for details). The crevice couple formed by the cathodic polarization curve in low level chlorinated seawater, adjusted for an area of 100 cm^2, and the anodic polarization curve generated in the aggressive propagation environment is presented in Figure 13. This mixed potential analysis reveals that the diffusion controlled limiting current density is, again, the driving force for crevice corrosion propagation. The hydrogen evolution reaction crosses the anodic curve at a current approximately 1 order of magnitude lower than the HOBr/OBr^- limiting current density and, therefore, contributes little to crevice

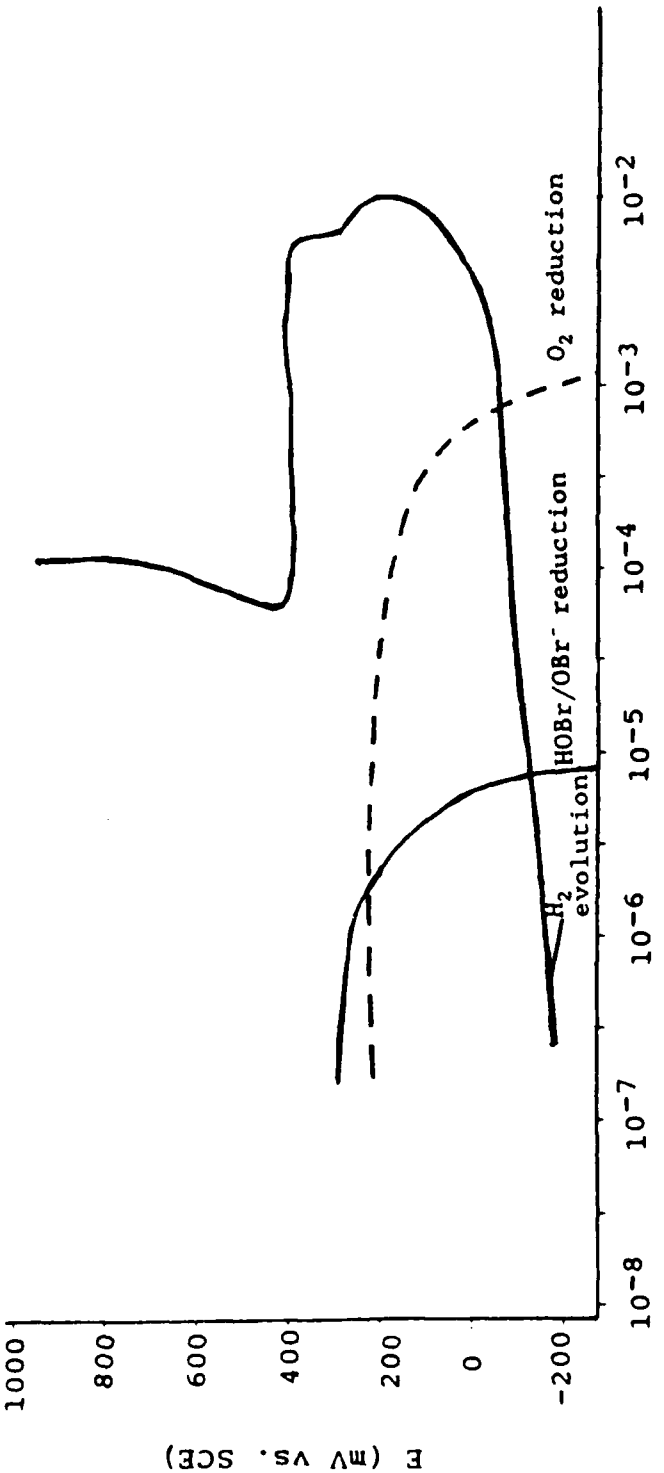

Figure 13 - Mixed Potential Analysis of the Crevice Couple in Low Level Chlorinated Seawater During the Propagation Stage (Natural Seawater Curve - Dashed Line)

corrosion propagation. In the chlorinated case the limiting current density for the reduction of HOBr/OBr^- is 2 orders of magnitude lower than the limiting current density for dissolved oxygen in the natural seawater environment (dashed line Figure 13) and is responsible for the lower crevice corrosion propagation rates observed in low level chlorinated seawater. Again, the IR drop down the length of the crevice would serve to decrease crevice corrosion propagation rates with increasing depth into the crevice. The lower limiting current density in the chlorinated case is attributed to the lower diffusion coefficient for HOBr in comparison to dissolved oxygen, to the fact that 2 electrons are transferred in the overall reduction of HOBr instead of the 4 electrons needed for dissolved oxygen, and to the lower concentration of oxidant (1 mg/l) in the potential region of interest in the chlorinated case than in the natural seawater case (8 mg/l).

CONCLUSIONS

1. An IR induced mechanism for crevice corrosion initiation has been characterized. Three distinctly different cases of this mechanism were identified and supported.

2. In natural seawater it has been shown that crevice corrosion initiates on alloy 625 by an IR induced mechanism.

3. The open circuit potential for alloy 625 shifts positively in natural seawater as a result of the formation of a bacterial slime film on the surface of the metal. This slime film effects the kinetics of the oxygen reduction reaction resulting in much higher crevice corrosion rates in natural versus artificial environments and emphasizes the importance of using natural seawater in lieu of artificial seawater for determining corrosion propagation rates.

4. After crevice corrosion initiation and before steady state propagation the acidity and chloride ion content of the crevice solution continue to increase, resulting in the formation of a large active nose in

the anodic polarization curve. It is the intersection of the diffusion controlled portion of the cathodic curve in the bulk environment and this active nose(incorporating the effects of IR) that drives crevice corrosion propagation.

5. Polarization experiments in a highly concentrated chloride solution rule out the possibility of crevice corrosion initiation on alloy 625 in chlorinated seawater by a breakdown mechanism. In this environment crevice corrosion initiates either as a result of an IR induced mechanism or an acidification mechanism.

6. A mixed potential analysis of the crevice couples in natural and chlorinated seawater reveals that the diffusion controlled portion of the $HOBr/OBr^-$ reduction reaction has a limiting current density 2 orders of magnitude lower than the limiting current density for oxygen reduction in natural seawater; thus explaining the lower propagation rates observed for this alloy in low level chlorinated seawater.

REFERENCES

1. F.N. Speller and F.L. LaQue, Corrosion, **6**, 209 (1950).

2. D.J. DePaul, Corrosion, **13**, 91 (1957).

3. E.V. Kunkel, Corrosion, **10**,260 (1954).

4. J.A. Collins, Corrosion, **11**, 27 (1955).

5. H.P. Hack, Mat.. Perf., **22**, 24 (1983).

6. A.P. Bond and H.J. Dundas, Mat. Perf., **23**, 39 (1984).

7. M.A. Streicher, Mat. Perf., **22**, 37 (1983).

8. N.G. Feige and R.L. Kane, Mat. Perf., **9**, 13 (1970).

9. L.W.Gleekman, Mat. Prot., **6**, 22 (1967).

10. L.W. Gleekman, Localized Corrosion, (Ed. K.W. Staehle), p.669. National Association of Corrosion Engineers, Houston (1974).

11. R.S. Sheppard, D.R. Hise, P.J. Gegner and W.L. Wilson, Corrosion, **18**, 211t (1962).

12. L.S. Remerski, J.J. Eckenrod, and C.W. Kovach, Corrosion, **39**, 31 (1983).

13. I.L. Rosenfeld, Localized Corrosion, (ed. K.W. Staehle), p.373. National Association of Corrosion Engineers, Houston (1974).

14. L.W. Gleekman, Corrosion, **14**, 21 (1958).

15. W.D. France, Localized Corrosion - Cause of Metal Failure, STP 516, p.164, American Society for Testing and Materials, Philadelphia (1972).

16. U.R. Evans, The Corrosion of Metals, p.93, Arnold, London (1926).

17. J.M. West, Elecrodepostion and Corrosion Processes, p.55. Van Nostrand, London (1965).

18. U.R. Evans, An Introduction to Metallic Corrosion, p.52. Arnold, London (1948).

19. I.L. Rosenfeld and I..K. Marshakov, Corrosion, **20**, 115t (1964).

20. J.R. Myers and M.F. Obrecht, 27th Annual Conf., National Association of Corrosion Engineers, paper 90, Chicago (1971).

21. M.G. Fontana and N.D.Greene, Corrosion Engineering, p.41. Mc Graw-Hill, New York (1967).

22. J.W. Oldfield and W.H. Sutton, Br. Corrso. J., **13**, 13 (1978).

23. M.H. Peterson, T.J. Lennox, and R.E Groover, Mat. Prot., **9**, 23 (1970).

24. T. Suzuki, M. Yambe and Y. Kitamura, Corrosion, **29**, 18 (1973)

25. F.D. Bogar and C.T. Fujii, Naval Research Laboratory Report 7690, March 1974.

26. A. Turnbull and M.K Gardner, Br. Corros. J., **16**, 140 (1981).

27. J.W. Oldfield and W.H. Sutton, Br. Corros. J., **15**, 31 (1980).

28. M.D. Carpenter, R. Francis, L.M. Phillips, and J.W. Oldfield, Br. Corros. J., **21**, 45 (1986).

29. P.O. Gartland, Corrosion 88, St. Louis, Research Symposium Abstract (1988).

30. B.E. Wilde and E. Williams, Elec. Acta, **16**, 1972 (1971).

31. J.M. Kroughman and F.P.Ijsseling, Proceedings of the Fifth International Congress on Marine Corrosion and Fouling, Barcelona, Spain, p. 214, (1980).

32. R.M. Kain and T.S. Lee, Laboratory Tests and Standards, ASTM STP 866, American Society for Testing and Materials, Philadelphia, p.299, (1983).

33. J.L. Dawson and M.G.S. Ferreira, Corr. Sci., **26**, 1027 (1986).

34. I.L. Rosenfeld and I..K. Marshakov, Corrosion, **20**, 115t (1964).

35. H.W. Pickering, Corrosion, **42**, 125 (1986).

36. A. Mollica and U.Montini, Rapporto Tecnico 2E/74, Istituto per la Corrosione Marina dei Metalli. Consiglio Nazionale delle Ricerche, Genova (1974).

37. A. Mollica and A. Trevis, Proceedings of the 4th International Congress on Marine Corrosion and Fouling, Juan-les-Pins, p.351 (1976).

38. J.M. Kroughman and F.P. Ijsseling, Proceedings of the Fifth International Congress on Marine Corrosion and Fouling, Barcelona, p.214 (1980).

39. S. Dexter, Corrosion 87, San Francisco, National Association of Corrosion Engineers, paper 377, (1987).

40. B. Johansen, P.O. Gartland, A. Supphellen, R. Tunold, 10th Scandinavian Corrosion Congress, Paper 27 (1986).

41. R.J. Ferrara, L.E. Taschenberg and P.J. Moran, Corrosion 85, Boston, National Assocaition of Corrosion Engineers, paper 211, (1985).

42. B.Wallen and S.Henrikson, Corrosion 88, St. Louis, National Association of Corrosion Engineers, paper 403, (1988).

43. R.L. Jolley and J.H. Carpenter, Water Chlorination: Environmental Impact and Health Effects, Vol. 4, Ann Arbor Science, p.3 (1983)

44. P.A. Klein and R.J. Ferrara, Crevice Corrosion of Nickel-Chromium-Molybdenum Alloys in Natural and Chlorinated Seawater, Corrosion 89, New Orleans (1989).

45. E.Bardal, R. Johnsen, P.O.Gartland, J.M. Drugli, Proceedings of the 10th Scandinavian Corrosion Congress, p. 7, Stochholm, (1986).

46. N.D. Greene, W.D.France, Jr., and B.E. Wilde, Corrosion, **21**, 275 (1965).

47. H.W. Pickering and R.P. Frankenthal,

J. Electrochem. Soc., **119**, 1297 (1972)

48. T.S. Lee, Electrochemical Corrosion Testing - ASTM STP 727, American Society for Testing and Materials, Baltimore, 1981.

49. H.W. Pickering, Joint United States - German Meeting on Electrochemical Passivity, to be published in Corr. Sci.

50. H.W. Pickering, Proceedings International Conference on Localized Corrosion, (Ed. H. Isaacs), National Association of Corrosion Engineers, Houston, to be published.

51. A. Valdes and H.W. Pickering, Proceedings International Conference on Localized Corrosion, (Ed. H. Isaacs), National Association of Corrosion Engineers, Houston, to be published.

52. A. Valdes and H.W. Pickering, Environmental Degradation of Engineering Materials III,(Ed. M.R. Louthan, Jr.), p.227. The Pennsylvania State University (1987).

53. G. Karlberg and G. Wraglen, Corr. Sci., **11**, 499 (1971).

54. F.P. Ijsseling, Br. Corros. J., **15**, 51 (1980).

55. H.W. Pickering and R.P. Frankenthal, J. Electrochem. Soc., **119**, 1304 (1972).

56. H.W. Pickering and R.P. Frankenthal, Localized Corrosion (ed. K.W. Staehle), p. 261. National Association of Corrosion Engineers, Houston (1974).

57. M.G. Fontana and N.D. Greene, Corrosion Engineering, Mc Graw-Hill, New York, p.336, (1978).

58. U.R.Evans, The Corrosion and Oxidation of Metals: Scientific Principles and Practical Applications, p.328. Arnold (1960).

59. G. Bombara, Corr. Sci., **9**, 519 (1969).

60. P.M. Strocchi, D. Sinigaglia, and D. Vicentini, Elec. Met., **2**, 38 (1967).

61. W.D. France, Jr. and N.D. Greene, Jr., Corrosion, **24**, 247 (1968).

62. R.C. Scarberry, E.L. Hibner and J.R. Crum, Paper 245 - Corrosion 79, National Association of Corrosion Engineers, Houston, (1979).

63. S.C. Tjong, Metals Forum, 7, 251 (1984).

64. W.K. Boyd and F.W. Fink, Corrosion of Metal in Marine Environments, Metals and Ceramics Information Center report 78-37, p. 38. (1978).

65. W. Z. Friend, Corrosion of Nickel and Nickel-Base Alloys, John Wiley & Sons, New York, p. 12. (1980).

66. J.R. Crum, Metals Handbook, Volume 13, p.654. ASM International, Metals Park (1987).

67. Metals Handbook, Desk Edition, p. 15.24. American Society for Metals, Metals Park, (1985).

68. D.B. Anderson, Galvanic Corrosion and Pitting - ASTM STP 576, American Society for Testing and Materials, Philadelphia, p.231 (1976).

69. R.M. Kain, Corrosion 86, Houston, National Association of Corrosion Engineers, paper 229, (1986).

70. R. M. Kain, private communication, April 1988.

71. H.Kaesche, Metallic Corrosion, p. 225, National Association for Corrosion Engineers, Houston (1985).

72. J.R. Meyers, F.H. Beck and M.G. Fontana, Corrosion, **21**, 277 (1965).

73. N. Sato, Passivity of Metals, (R.P.Frankenthal and J. Kruger eds.), p.30, The Electrochemical Society, Princeton (1978).

74. R.M. Kain, Metals Handbook, Vol. 13, p.111. ASM International, Metals Park (1987).

75. R.M. Kain, private communication, Sept 1988.

BASIC DISTRIBUTION LIST

Technical and Summary Reports 1988

Organization	Copies
Defense Documentation Center Camerson Station Alexandria, VA 22314	12
Office of Naval Research Dept. of the Navy 800 N. Quincy Street Arlington, VA 22217 Attn: Code 1131	3
Naval Research Laboratory Washington, DC 20375 ATTN: Codes 6000 6300 2627	
Naval Air Development Center Code 606 Warminister, PA 18974 ATTN: Dr. J. DeLuccia	
Commanding Officer Naval Surface Weapons Center White Oak Laboratory Silver Spring, MD 20910 ATTN: Library	1
Naval Oceans Systems Center San Diego, CA 92132 ATTN: Library	1
Naval Postgraduate School Monterey, CA 93940 ATTN: Mechanical Engineering Department	1
Naval Air Systems Command Washington, DC 20360 Attn: Code 310A Code 5304B Code 931A	1 1 1
Naval Sea System Command Washington, DC 20362 ATTN: Code 05M Code 05R	1 1
Naval Air Prop. Test Ctr. Trenton, NY 08628 ATTN: Library	1
Naval Contruction Battallion Civil Engineering Laboratory Port Hueneme, CA 93043 ATTN: Materials Div.	1
Naval Electronics Laboratory San Diego, CA 92152 ATTN: Electron Materials Sciences Division	1
Naval Missile Center Materials Consultant Code 3312-1 Point Mugu, CA 92041	1
Commander David Taylor Research Center Bethesda, MD 20084	1
Naval Underwater System Ctr. Newport, RI 02840 ATTN: Library	1
Naval Weapons Center China Lake, CA 93555 ATTN: Library	1
NASA Lewis Research Center 21000 Brookpark Road Cleveland, OH 44135 ATTN: Library	1
National Bureau of Standards Gaithersburg, MD 20899 Attn: Metallurgy Division Ceramics Division Fracture & Deformation Division	1 1 1

Naval Facilities Engineering
Command
Alexandria, VA 22331
ATTN: Code 03 1

Scientific Advisor
Commandant of the Marine Corps
Washington, DC 20380
ATTN: Code AX 1

Army Research Office
P.O. Box 12211
Research Triangle Park, NC 27709
ATTN: Metallurgy & Ceramics
Program 1

Army Materials and Mechanics
Research Center
Watertown, MA 02172
ATTN: Research Programs Office 1

Air Force Office of Scientific
Research/NE
Building 410
Bolling Air Force Base
Washington, DC 20332
ATTN: Electronics & Materials
Science Directorate 1

NASA Headquarters
Washington, DC 20546
Attn: Code RM 1

Defense Metals & Ceramics
Information Center
Battelle Memorial Inst.
505 King Avenue
Columbus, OH 43201 1

Metals and Ceramics Div.
Oak Ridge National Laboratory
P.O. Box X
Oak Ridge, TN 37380 1

Los Alamos Scientific Lab.
P.O. Box 1663
Los Alamos, NM 87544
ATTN: Report Librarian 1

Argonne National Laboratory
Metallurgy Division
P.O. Box 229
Lemont, IL 60439 1

Brookhaven National Laboratory
Technical Information Division
Upton, Long Island
New York 11973
Attn: Research Library 1

Lawrence Radiation Lab.
Library
Building 50, Room 134
Berkely, CA 1

David Taylor Research Ctr
Annapolis, MD 21402-5067
ATTN: Code 281 1
Code 2813 1
Code 0115 1

RE/1131/88/75
4315 (036)

Supplemental Distribution List Feb 1988

Prof. I.M. Bernstein
Illinois Institute of Technology
IIT Center
Chicago, Ill 60615

Prof. H.K. Birnbaum
Dept. of Metallurgy & Mining Eng.
University of Illinois
Urbana, Ill 61801

Prof. H.W. Pickering
Dept. of Materials Science and Eng.
The Pennsylvania State University
University Park, PA 16802

Prof. D.J. Duquette
Dept. of Metallurgical Eng.
Rensselaer Polytechnic Inst.
Troy, NY 12181

Prof. J.P. Hirth
Dept. of Metallurgical Eng.
The Ohio State University
116 West 19th Avenue
Columbus, OH 43210-1179

Prof. H. Leidheiser, Jr.
Center for Coatings and Surface Research
Sinclair Laboratory, Bld. No. 7
Lehigh University
Bethlehem, PA 18015

Dr. M. Kendig
Rockwell International Science Center
1049 Camino Dos Rios
P.O. Box 1085
Thousand Oaks, CA 91360

Prof. R. A. Rapp
Dept. of Metallurgical Eng.
The Ohio State University
116 West 19th Avenue
Columbus, OH 43210-1179

Profs. G.H. Meier and F.S.Pettit
Dept. of Metallurgical and
Materials Eng.
University of Pittsburgh
Pittsburgh, PA 15261

Dr. W. C. Moshier
Martin Marietta Laboratories
1450 South Rolling Rd.
Baltimore, MD 21227-3898

Prof. P.J. Moran
Dept. of Materials Science & Eng.
The Johns Hopkins University
Baltimore, MD 21218

Prof. J. Kruger
Dept. of Materials Science & Eng.
The Johns Hopkins University
Baltimore, MD 21218

Prof. R.P. Wei
Dept. of Mechanical Engineering
and Mechanics
Lehigh University
Bethlehem, PA 18015

Prof. W.H. Hartt
Department of Ocean Engineering
Florida Atlantic University
Boca Raton, Florida 33431

Dr. B.G. Pound
SRI International
333 Ravenswood Ave.
Menlo Park, CA 94025

Prof. C.R. Clayton
Department of Materials Science
& Engineering
State University of New York
Stony Brook
Long Island, New York 11794

Prof. Boris D. Cahan
Dept. of Chemistry
Case Western Reserve Univ.
Cleveland, Ohio 44106

Dr. K. Sadananda
Code 6323
Naval Research Laboratory
Washington, D.C. 20375

Prof. M.E. Orazem
Dept. of Chemical Engineering
University of Virginia
Charlottesville, VA 22901

Dr. G.R. Yoder
Code 6384
Naval Research Laboratory
Washington, D.C. 20375

Dr. N. S. Bornstein
United Technologies Research Center
East Hartford, CT 06108

Dr. A.L. Moran
Code 2812
David Taylor Research Center
Annapolis, MD 21402-5067

Dr. B.E. Wilde
Dept. of Metallurgical Engineering
The Ohio State University
116 West 19th Avenue
Columbus, OH 43210-1179

Prof. G.R. St. Pierre
Dept. of Metallurgical Eng.
The Ohio State University
116 West 19th Avenue
Columbus, OH 43210-1179

Prof. G. Simkovich
Dept. of Materials Science & Eng.
The Pennsylvania State University
University Park, PA 16802

Dr. E. McCafferty
Code 6322
Naval Research Laboratory
Washington, D. C. 20375

Dr. J.A. Sprague
Code 4672
Naval Research Laboratory
Washington, D.C. 20375

Dr. C.M. Gilmore
The George Washington University
School of Engineering & Applied Science
Washington, D.C. 20052

Dr. F.B. Mansfeld
Dept. of Materials Science
University of Southern California
University Park
Los Angeles, CA 90089

Dr. Ulrich Stimming
Dept. of Chemical Eng. & Applied Chemistry
Columbia University
New York, N.Y. 10027

Prof. J. O'M. Bockris
Dept. of Chemistry
Texas A & M University
College Station, TX 77843